Mon. Not. R. Astron. Soc. **000**, 1–5 (2014) Printed 4 March 2014 (MN LATEX style file v2.2)

Chaotic enhancement of dark matter density in binary systems and galaxies

G. Rollin[1⋆] J. Lages[1] and D. L. Shepelyansky[2]
[1] *Institut UTINAM, Observatoire des Sciences de l'Univers THETA, CNRS & Université de Franche-Comté, 25030 Besançon, France*
[2] *Laboratoire de Physique Théorique du CNRS, IRSAMC, Université de Toulouse, UPS, F-31062 Toulouse, France*

Accepted 2014 December XX. Received 2014 March XX; in original form 2014 March 2

ABSTRACT
Using symplectic map description we study the capture of galactic dark matter particles (DMP) in two-body and few-body galaxies. This approach allows to model scattering of 10^{16} DMP following time evolution of captured particle on about 10^9 orbital periods. We obtain DMP density distribution inside such galaxies and determine the enhancement factor of their density in galactic center compared to its inter-galactic value as a function of mass ratio of galactic bodies and a ratio of body velocity to velocity of galactic DMP wind. We find that the enhancement factor can be of the order of ten thousands.

Key words: dark matter, Solar System, Hamiltonian chaos, dynamical maps

1 INTRODUCTION

The capture process of galactic wind of dark matter particles (DMP) by binary systems is directly related to the three-body problem which dynamics is generally non-integrable as it had been proved by Poincaré (1890). The analysis of velocity curves in galaxies started by Zwicky (1933); Ruben *et al.* (1980) had led to a conclusion about dominance of dark matter in the Universe (see e.g. Bertone *et al.* (2005); Merritt (2010); Garrett and Dũda (2011)). There are also serious indications that the volume density ρ_v of DMP in the center of galaxies is enhanced by four-five orders of magnitude compared to its inter-galactic value (see e.g. Garrett and Dũda (2011)). Two main scenarios of this enhancement are possible: in the first one galaxies are born in spots of high DMP density, while in the second one galaxies capture DMP and accumulate it inside them. Here we consider the second scenario analyzing a capture process of DMP galactic wind in a simplified galaxy model represented by a binary system with a massive star in the center and a light body rotating around. It can be the Sun and a planet like Jupiter, or a super massive black hole (SMBH) and a light star or BH.

There are certain signs that a strong density enhancement is possible in our simplified galaxy model. Indeed, recent studies by Khriplovich and Shepelyansky (2009); Lages and Shepelyansky (2013) showed that the capture cross-section σ diverges at low energies being much larger than the area of Jupiter orbit around the Sun. Also it is shown by Lages and Shepelyansky (2013) that a density of captured DMP on a distance of Jupiter radius $r < r_p = r_J$ is enhanced by a factor $\zeta \approx 4000$ compared to the galactic DMP density, taken in a typical energy range which is captured after one orbital period of DMP around the Sun corresponding to velocities $v < v_{cap} \sim v_p\sqrt{m_p/M} \sim 1km/s \ll u$. Here, m_p, M are masses of light and massive bodies, $u \approx 220km/s$ is an average velocity of galactic DMP wind for which, following Bertone *et al.* (2005), we assume a Maxwell velocity distribution $f(v)dv = \sqrt{54/\pi}v^2/u^3 \exp(-3v^2/2u^2)dv$. Thus we can expect that for a SMBH binary system with $v_{cap} > u$ there is a large enhancement factor ζ_g of galactic captured DMP density $\rho_g \sim 4 \times 10^{-25} g/cm^3$, compared to its typical inter-galactic value $\rho_{g0} \sim 10^{-29} g/cm^3$.

2 SYMPLECTIC MAP DESCRIPTION

Following the approach developed by Petrosky (1986); Chirikov and Vecheslavov (1989); Malyshkin and Tremaine (1999); Lages and Shepelyansky (2013) we use a symplectic dark map description of the dynamics of DMP on one orbital period in a binary system:

$$w_{n+1} = w_n + F(x_n)\ , \quad x_{n+1} = x_n + w_{n+1}^{-3/2}\ , \qquad (1)$$

where $x_n = t_n/T_p\ (mod\ 1)$ is given by time t_n taken at the moment of DMP $n-th$ passage through perihelion, T_p is the planet period and $w = -2E/m_d v_p^2$. Here E, m_d, v_p are respectively energy, mass of DMP and velocity of planet/star. The amplitude J of kick F-function is proportional to the mass ratio $J \sim m_p/M$. The shape of $F(x)$ depends on DMP perihelion distance q, inclination angle θ between the planetary plane (x, y) and DMP plane, and perihelion orientation

⋆ E-mail: rollin(at)obs-besancon.fr (RG)

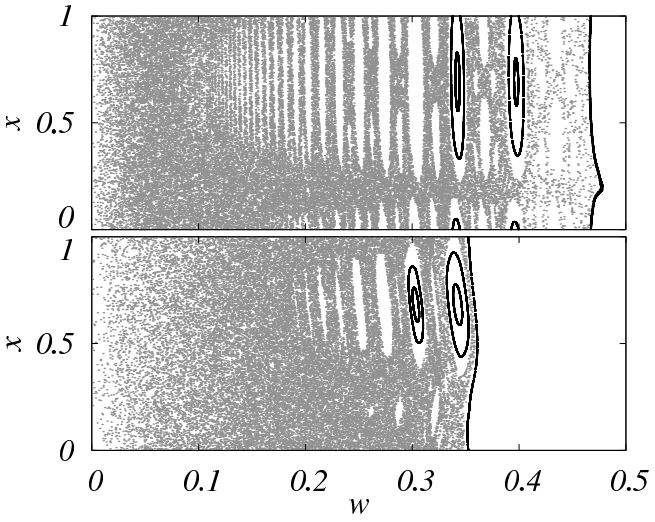

Figure 1. Poincaré sections for the dark map (1) (top) and the Kepler map (2) (bottom) for parameters of the Halley comet case in (1) and $J = 0.007$ in (2) (see text).

angle φ as discussed by Lages and Shepelyansky (2013). In the following we use units with $m_d = v_p = r_p = 1$.

For $q > r_p$ the amplitude J drops exponentially with q and $F(x) = J\sin(2\pi x)$ as shown by Petrosky (1986). This functional form of $F(x)$ is significantly simpler than the real one at $q < r_p$ while it still produces a chaotic dynamics at $|w| \ll 1$ and integrable motion with invariant curves above a chaos border $w > w_{ch}$. In this regime the map takes the form

$$w_{n+1} = w_n + J\sin(2\pi x_n)\ , \quad x_{n+1} = x_n + w_{n+1}^{-3/2}\ . \qquad (2)$$

The same map describes a microwave ionization of excited hydrogen atoms being called the Kepler map (see Casati *et al.* (1987); Shepelyansky (2012)). There, the Coulomb attraction plays the role of gravity while a circular planet rotation is effectively created by a microwave polarization. The microwave ionization experiments, performed by Galvez *et al.* (1988), are done for 3-dimensional atoms but still the ionization process is well described by the Kepler map (see Casati *et al.* (1990); Shepelyansky (2012)). These results provide additional arguments in favor of a simplified Kepler map description of DMP dynamics in binary systems.

The similarity of dynamics of dark (1) and Kepler (2) maps is also well visible from comparison of their Poincaré sections shown in Fig 1 for the typical dark map parameters corresponding to the Halley comet (see Fig.1a at Lages and Shepelyansky (2013)) and a corresponding parameter J of the Kepler map.

To take into account that J decreases with q we use the relation $J = J_0 = const$ for $q < q_b$ and $J = J_0\exp(-\alpha(q - q_b)))$ for $q \geqslant q_b$ (below J is used instead of J_0). We use $q_b = 1.5$ and $\alpha = 2.5$, corresponding to typical dark map parameters (see Fig.1 at Lages and Shepelyansky (2013)), but we checked that the obtained enhancement is not affected by a moderate variation of q_b, α. The simplicity of map (2) allows to increase a number N_p of injected DMP by a factor hundred compared to map (1). The correspondence between (1) and (2) is established by the relation $J = 5m_p/M$ which works approximately for the typical parameters of Halley comet case.

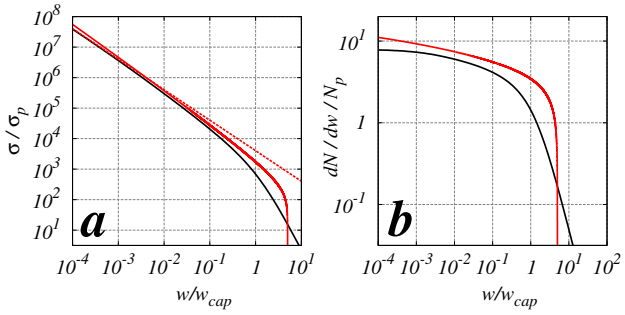

Figure 2. *(a)* Dependence of capture cross-section σ on DMP energy w for Sun-Jupiter (black curve, data by Lages and Shepelyansky (2013)) and for the Kepler map at $J = 0.005$ (red curve); a dashed line shows dependence $\sigma \propto 1/|w|$. *(b)* Dependence of rescaled captured number of DMP on energy w for the models of left panel. Here $w_{cap} = 0.001$.

Of course, as discussed by Lages and Shepelyansky (2013), the dark map and moreover the Kepler map give an approximate description of DMP dynamics in binary systems. However, this approach is much more efficient compared to exact solution of Newton equations used by Peter (2009); Sivertsson and Edsjö (2012) and allows to obtain results with enormous number of DMP injected during the life time of Solar System (SS) $t_S = 4.5 \times 10^9 years$. The validity of such a map description is justified by results obtained by Petrosky (1986); Chirikov and Vecheslavov (1989); Malyshkin and Tremaine (1999); Lages and Shepelyansky (2013); Casati *et al.* (1990).

3 CAPTURE CROSS-SECTION

The capture cross-section σ is computed as previously described by Lages and Shepelyansky (2013) with $\sigma(w)/\sigma_p = (\pi^2 r_p|w|)^{-1}\int_0^{2\pi} d\theta \int_0^{\pi} d\varphi \int_0^{\infty} dq h(q,\theta,\varphi)$, where h is a fraction of DMP captured after one map iteration from $w < 0$ to $w > 0$, given by an interval length inside $F(x)$ envelope at $|w| = const$, $\sigma_p = \pi r_p^2$. The equation for $\sigma(w)$ is based on the expression for the scattering impact parameter $r_d^2 = 2qr_p/|w|$. For the Kepler map $h-$function depends only on q and numerical computation is straightforward. The differential energy distribution of captured DMP is $dN/dw = \sigma(w)n_g f(w)/2$ with $n_g = \rho_g/m_d$.

The results for $\sigma(\omega)$ and $dN/dw/N_p$, obtained for maps (1) and (2), are shown in Fig. 2. Here $N_p = \int_0^1 dw n_g \sigma_p v_p^2 f(w)/2$ is a number of DMP crossing the planet orbit area per unit of time. The results of Fig. 2 show that both maps give similar results that provides an additional support for the Kepler map description. The theoretical dependence $\sigma \propto 1/|w|$, predicted by Khriplovich and Shepelyansky (2009), is well confirmed. The only difference between two maps is a restriction $|w| \leqslant J$ for (2) since it has a finite kick amplitude while for (1) some orbits can be captured with $|w| > J = 5m_p/M$ due to close encounters. However, the probability of such events is small.

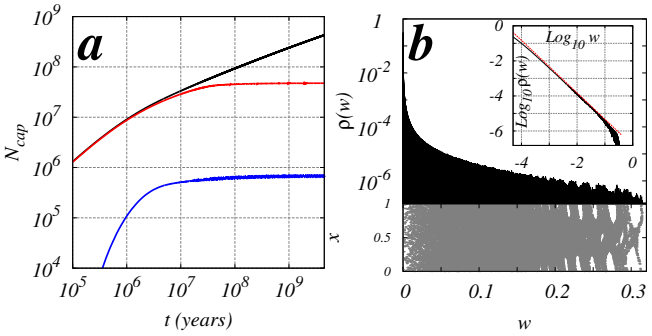

Figure 3. *(a)* The number N_{cap} of captured DMP as a function of time t in years for energy range $w > 0$ (black curve), $w > 4 \cdot 10^{-5}$ corresponding to half distance between Sun and Alpha Centauri System (red curve), $w > 1/20$ corresponding to $r < 100AU$ (blue curve); $N_J = 4 \times 10^{11}$ DMP are injected during SS life time t_S; data are obtained from the map (2) at $J = 0.005$, $u = 17$ corresponding to Sun-Jupiter case. *(b)* Top part shows density distribution $\rho(w) \propto dN/dw$ in energy at time t_S (normalized as $\int_0^\infty \rho dw = 1$), bottom part shows the Poincaré section of the map (2); inset shows density distribution of captured DMP in w (black curve), a red line shows a slope -3/2.

4 CHAOTIC DYNAMICS

The injection, capture, evolution and escape of DMP is computed as described by Lages and Shepelyansky (2013): we model numerically a constant flow of scattered DMP with energy distribution $dN_s = \sigma(w) v_p^2 f(w) dw/2$ per time unit (we use $q \leqslant q_{max} = 4r_p$). For Jupiter we have $u \approx 17 \gg 1$ and $dN_s \propto dqdw$. However, for SMBH we can have $u^2 < J$ so that one kick captures almost all DMP from galactic distribution $f(w)$. In such a case we use the whole distribution $f(w)$ ($w = v^2$). The map (2) is simpler than (1) since the kick function depends only on q that allows to perform simulations with a larger number of DMP.

The scattering and evolution processes are followed during the whole life time t_S of SS. The total number of DMP, injected during time t_S for $|w| \leqslant J$ and all q is N_J. For the Kepler map a maximum value is $N_J = 4 \times 10^{11}$ being 100 times larger than for the dark map.

The time dependence $N_{cap}(t)$ for the Kepler map, shown in Fig. 3, is very similar to those found for the dark map by Lages and Shepelyansky (2013). For a finite SS region $w > 1/20$ the growth of $N_{cap}(t)$ saturates after a time scale $t_d \approx 10^7 years$. This scale approximately corresponds to a diffusive escape time $t_d \sim 12 years/D \sim 10^6 years$ where the diffusion rate is taken in a random phase approximation $D \approx J^2/2$ (see e.g. Casati *et al.* (1987)). The diffusive spreading goes from $w \sim 0$ up to chaos border $w_{ch} \approx 0.3$. This value is in a good agreement with the theoretical value $w_{ch} = (3\pi J)^{2/5} = 0.29$ obtained from the Chirikov criterion Chirikov (1979) by Petrosky (1986); Casati *et al.* (1987); Khriplovich and Shepelyansky (2009). As for the dark map we obtain density distribution $\rho(w) \propto 1/w^{3/2}$ corresponding to the ergodic estimate according to which $\rho(w)$ is proportional to time period at a given w. The results of Figs. 1,2,3 confirm a close similarity of dynamics described by maps (1) and (2).

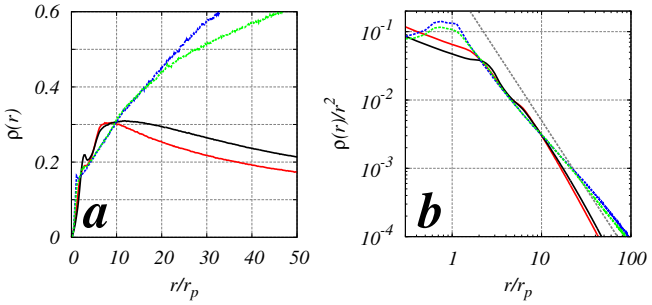

Figure 4. (a) Stationary radial density $\rho(r) \propto dN/dr$ from the Kepler map at $J = 0.005$ with $u = 17$ at time t_S (red curve) and $u = 0.035$ at time $t_u \approx 4 \times 10^8 T_p$(black curve); data from the dark map at $m_p/M = 10^{-3}$ are shown by the blue curve at $u = 17$ and time t_S for the Sun-Jupiter case, and by the green curve at $u = 0.035$ and t_S for the SMBH; the normalization is fixed as $\int_0^{6r_p} \rho dr = 1$, $r_p = 1$. *(b)* Volume density $\rho_v = \rho/r^2$ from the data of panel *(a)*, the dashed line shows the slope -2.

5 RADIAL VARIATION OF DARK MATTER DENSITY

To compute the DMP density we consider captured orbits N_{AC} with $w > 4 \times 10^{-5}$. The radial density $\rho(r)$ is computed by the method described by Lages and Shepelyansky (2013): N_{AC} are determined at instant time t_S, for them the dynamics in real space is recomputed during a time period $\Delta t \sim 100$ years of planet. The value of $\rho(r)$ is computed by averaging over $k = 10^3$ points randomly distributed over Δt for all N_{AC} orbits. We also checked that a semi-analytical averaging, using exact density distribution over Kepler ellipses for each of N_{AC} orbits, gives the same result. From obtained space distribution we determine a fraction η_{r_i} of N_{AC} DMP orbits located inside a range $0 \leqslant r \leqslant r_i$ by computing $\eta_{r_i} = \Delta N_i/(kN_{AC})$ where ΔN_i is a number of points inside the above range (we use $r_i/r_p = 0.2, 1, 6$).

In Fig. 4 we show the dependence of radial $\rho(r)$ and volume $\rho_v = \rho/r^2$ densities on distance r. For the Kepler map data the density $\rho(r)$ has a characteristic maximum at r_{max} which is determined by the chaos border position $r_{max} \approx 2/w_{ch}$ (this dependence, as well as the relation $w_{ch} = (3\pi J)^{2/5}$, is numerically confirmed for the studied range $10^{-3} < J < 10^{-2}$). The density profile $\rho(r)$ is not sensitive to the value of u remaining practically without change for $u = 17,\ 0.035$. For the dark map a variation of the kick function with q and angles leads to a variation of w_{ch} that leads to a slow growth of ρ at large r. A power law fit of $\rho_v \propto 1/r^\beta$ in a range $2 < r < 100$ gives $\beta \approx 2.25 \pm 0.003$ for the Kepler map data and $\beta = 1.52 \pm 0.002$ for the dark map. We attribute the difference in β values to a larger fraction of integrable islands for the dark map as it is visible in Fig. 1 for typical parameters. We should note that an effective range of radial variation is bounded by kick amplitude with $r < r_{cap} \approx 1/J$ and in the range $r_p < r < r_{cap}$ the data are compatible with $\rho \sim const$ (dashed line in Fig. 4b).

We note that the value of u does not significantly affect the density variation with r as it is clearly seen from Fig. 4. Also the spacial density distribution from the dark map at $u = 0.035$ shown in Fig. 5 is very similar to those at $u = 17$ (see Fig.5 by Lages and Shepelyansky (2013)). Such an independence of u is due to the fact that $\rho(r)$ is determined

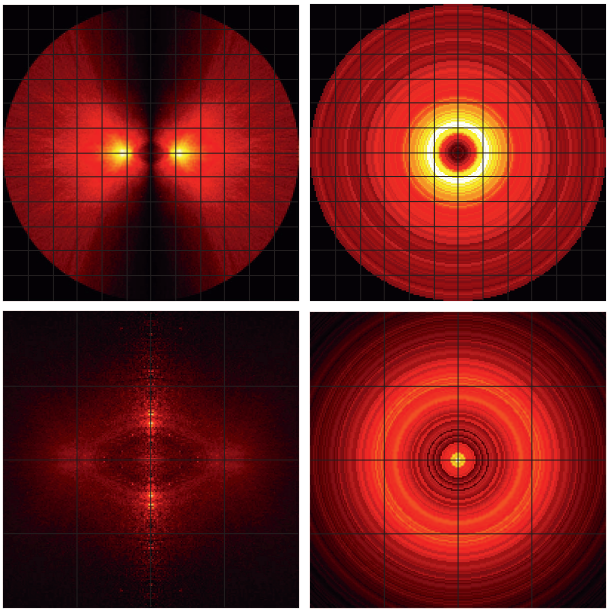

Figure 5. Density of captured DMP at present time $t_S/T_p = 4.5 \times 10^9$ for the dark map at $m_p/M = 10^{-3}$ and $u/v_p = 0.035$ *Top panels:* DMP surface density $\rho_s \propto dN/dzdr_\rho$ shown at *left* in cross plane $(0, y, z)$ perpendicular to planet orbit (data are averaged over $r_\rho = \sqrt{x^2+y^2} = const$), at *right* in planet plane $(x, y, 0)$; only the range $|r| \leqslant 6$ around the center is shown. *Bottom panels:* corresponding DMP volume density $\rho_v \propto dN/dxdydz$ at *left* in plane $(0, y, z)$, at *right* in planet plane $(x, y, 0)$; only the range $|r| \leqslant 2$ around SMBH is shown. Color is proportional to density with yellow/black for maximum/zero density.

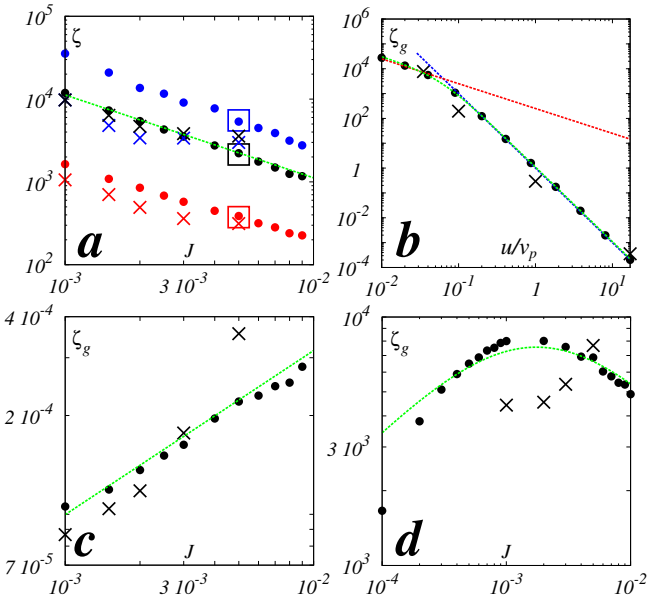

Figure 6. *(a)* Dependence of DMP density enhancement factor $\zeta = \rho_v(r_i)/\rho_{gJ}$ on J at $u/v_p = 17$ (Jupiter); here ρ_{gJ} is galactic DMP volume density for energy range $0 < |w| < J$ and $r_i = 0.2r_p, r_p, 6r_p$ (blue, black, red colors); points and squares show results for the map (2) with number of injected particles $N_J = 4 \times 10^9$ and 4×10^{11} respectively; crosses show data for the map (1) with $N_J = 4 \times 10^9$ and $J = 5m_p/M$. *(b)* Dependence of galactic enhancement factor $\zeta_g = \rho_v(r_i)/\rho_g$ on u/v_p at $r_\zeta = r_p$ and $J = 0.005$ in (2) (points) and $m_p/M = 0.001$ in (1) (crosses), here ρ_g is global galactic density; lines show dependencies $\zeta_g \propto 1/u$ (red) and $\zeta_g \propto 1/u^3$ (blue). *(c)* Dependence of ζ_g on J at $u/v_p = 17$; *(d)* the same at $u/v_p = 0.035$, parameters of symbols are as in *(a),(b)*. Green curve shows theory (3) in all panels.

by dynamics at $w > 0$ which is practically not sensitive to DMP energies at $-J < w < 0$ which are captured by one kick.

6 ENHANCEMENT OF DARK MATTER DENSITY

To determine the enhancement of DMP density captured by a binary system we follow the method developed by Lages and Shepelyansky (2013). We compute the total mass of DMP flow crossing the range $q \leqslant 4r_p$ during time t_S: $M_{tot} = \int_0^\infty dvvf(v)\sigma\rho_g t_S \approx 35\rho_g t_S k r_p M/u$ where we use the cross-section $\sigma = \pi r_d^2 = 8\pi k M r_p/v^2$ for injected orbits with $q \leqslant 4r_p$, $w = v^2$, k is the gravitational constant. For SS at $u/v_p \approx 17$ we have $M_{tot} \approx 0.5 \cdot 10^{-6} M$.

From the numerically known fractions η_{ri} of previous Section and the fraction of captured orbits $\eta_{AC} = N_{AC}/N_{tot}$ we find the mass $M_{ri} = \eta_{ri}\eta_{AC}M_{tot}$ inside the volume $V_i = 4\pi r_i^3/3$ of radius $r < r_i$ ($r_i = 0.2r_p; r_p; 6r_p$). Here N_{tot} is the total number of injected orbits during the time t_S while the number of orbits injected in the range $|w| < J$ (only those can be captured) is $N_J = N_{tot}(\int_0^J dwf(w)/w)/(\int_0^\infty dwf(w)/w)$. For $J \ll u^2$ we have $\kappa = N_{tot}/N_J = 2u^2/(3J) \approx 3.8 \times 10^4$ for $u/v_p = 17$ and $\kappa = 1$ for $u/v_p = 0.035$ at $J = 0.005$. Thus for $u/v_p = 17$ the number of orbits, injected at $0 < |w| < J$, $N_J = 4 \times 10^{11}$ corresponds to the total number of injected orbits $N_{tot} \approx 1.5 \times 10^{16}$. Finally we obtain the global density enhancement factor $\zeta_g(r_i) = \rho_v(r_i)/\rho_g \approx 16\pi\eta_{ri}\eta_{AC}(r_p/r_i)^3\tau_S v_p/u$, where $\tau_S = t_S/T_p$ is injection time expressed in number of planet periods $T_p = 2\pi r_p/v_p$. For $u^2 \gg J$ it is useful to determine the enhancement $\zeta = \rho_v(r_i)/\rho_{gJ}$ of scattered galactic density in the range $0 < |w| < J$ which density is $\rho_{gJ} \approx 1.38\rho_g J^{3/2}(v_p/u)^3$. Thus $\zeta = 0.72\zeta_g(u/v_p)^3/J^{3/2}$.

The results of DMP density enhancement factors ζ and ζ_g are shown in Fig. 6. At $(u/v_p)^2 \gg J$ we have $\zeta \gg 1$ and $\zeta_g \ll 1$. At $u/v_p = 17$ we find that $\zeta \propto 1/J$ (the fit gives exponent $a = 1.04 \pm 0.01$) and $\zeta_g \propto \sqrt{J}$ (the fit exponent is $a = 0.46 \pm 0.1$) in agreement with the above relation between ζ and ζ_g. In global we have $\zeta_g \propto 1/u$ for $u/v_p \ll \sqrt{J}$ and $\zeta_g \propto 1/u^3$ for $u/v_p \gg \sqrt{J}$. There is only weak variation of ζ_g with J for $u/v_p \ll \sqrt{J}$. The values of ζ and ζ_g have similar values for the dark and Kepler maps (a part of the fact that at $r_i = 0.2r_p$ and $r_i = r_p$ the dark map has approximately the same ζ since there $\rho_v(r) \sim const$ for $r \leqslant r_p$).

All these results can be summarized by the following formula for chaotic enhancement factor of DMP density in a binary system:

$$\zeta_g = A\sqrt{J}(v_p/u)^3/[1 + BJ(v_p/u)^2] \, , J = 5m_p/M \, . \qquad (3)$$

Here ζ_g is given for DMP density at $r_i = r_p$ and $A \approx 15.5$, $B \approx 0.7$. This formula gives a good description of numerical data of Fig. 6. For $u^2 \gg J$ we have $\zeta_g \ll 1$ but we still have enhancement $\zeta = 0.72\zeta_g(u/v_p)^3/J^{3/2} \approx 0.72A/J \gg 1$. The color representation of dependence (3) is shown in Fig. 7.

The formula (3) can be understood on the basis of sim-

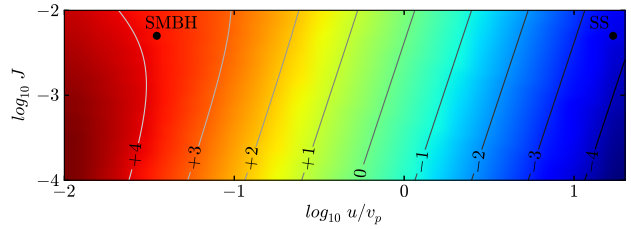

Figure 7. Logarithm of DMP density enhancement factor $\log_{10}\zeta_g$ from (3), shown by color and log value-levels, as a function of u/v_p and J; two points are for $J = 0.005$, $u/v_p = 17$ (SS) and $u/v_p = 0.035$ (SMBH; such v_p is about 2% of light velocity)).

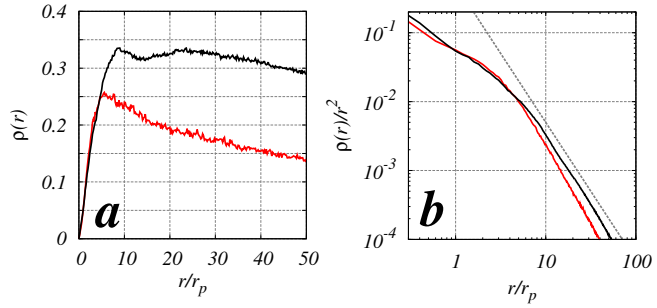

Figure 8. (a) Radial density $\rho(r) \propto dN/dr$ for the Kepler models of SS (red curve) and SMBH galaxy (black curve) at $t_S/T_p \approx 4 \times 10^8$; the normalization is fixed as $\int_0^{6r_p} \rho dr = 1$, $r_p = 1$ for fifth body. *(b)* Volume density $\rho_v = \rho/r^2$ from the data of *(a)*, the dashed line shows slope -2 (see text for details).

ple estimates. The total captured mass $M_{cap} \approx M_{AC}$ is accumulated during the diffusive time t_d and hence $M_{cap} \sim v_p^2 J t_d M_{tot}/(\pi u^2 t_S) \sim \rho_g \tau_d J (v_p/u)^3$ where $\tau_d = t_d/T_p$ and we omit numerical coefficients. This mass is concentrated inside a radius $r_{cap} \sim 1/J$ so that at $r \sim 1/J$ the volume density is $\rho_v(r = 1/J) \sim M_{cap}/r_{cap}^3 \sim \rho_g J^2 w_{ch}^2 (v_p/u)^3 \sim \rho_{gJ} J^{1/2} w_{ch}^2 \sim \rho_{gJ} J^{1.3}$, where we use a relation $\tau_d \sim w_{ch}^2/J^2 \sim 1/J^{6/5}$. (Our modeling of injection process in the Kepler map with a constant injection flow in time, counted in number of map iterations, indeed, shows that the number of absorbed particles scales as $N_K \sim \tau_d \sim J^{-6/5}$ at small J.) It is important to stress that $\rho_v(r = 1/J) \ll \rho_{gJ}$ in contrast to a naive expectation that $\rho_v(r = 1/J) \sim \rho_{gJ}$. Using our empirical density decay $\rho_v \propto 1/r^\beta$ with $\beta \approx 2.25$ for the Kepler map we obtain $\zeta \propto 1/J^{0.95}$ being close to the dependence $\zeta \sim 1/J$ and $\zeta_g \sim J^{1/2}/(u/v_p)^3$ from (3) at $u^2 \gg J$. For the dark map we have $\beta \approx 1.5$ but $w_{ch} \sim const$ due to sharp variation of $F(x)$ with x that again gives $\zeta \sim 1/J$. We think that it is difficult to obtain exact analytical derivation of the relation $\zeta \sim 1/J$ due to contributions of different q values (which have different τ_d) and different kick shapes in (1) that affect τ_d and the structure of chaotic component. In the regime $(u/v_p)^2 \ll J$ all energy range of scattering flow is absorbed by one kick and M_{cap} is increased by a factor $(u/v_p)^2/J$ leading to increase of ζ_g by the same factor giving $\zeta_g \propto v_p/(u\sqrt{J})$ in agreement with (3).

Above we considered the DMP capture in a two-body galaxy. Within the Kepler map approach it is easy to perform analysis for the whole SS (for a SMBH galaxy) including all 8 planets (8 stars) with given positions r_i and velocities v_i measured in units of orbit radius r_p and velocity v_p of Jupiter for SS at $u/v_p = 17$ (and of e.g. the fifth star for SMBH galaxy at $u/v_p = 0.035$). Thus in (2) we have now for the SS 8 kick terms with $J_i \sim (m_i/M)(v_i/v_p)^2$. For the SMBH galaxy model we consider 8 stars modeled by the map (2) with the values $J_1 = 2.5 \times 10^{-4}$, $J_2 = 5 \times 10^{-4}$, $J_3 = 7.5 \times 10^{-4}$, $J_4 = 10^{-3}$, $J_5 = 2.5 \times 10^{-3}$, $J_6 = 6.25 \times 10^{-4}$, $J_7 = 5 \times 10^{-4}$, $J_8 = 1.25 \times 10^{-4}$ with the same ration r_i/r_p as for the SS. In both cases we injected $N_J = 2.8 \times 10^{10}$ particles considering evolution during τ_S orbital periods of Jupiter (fifth star). The steady state density distribution is shown in Fig. 8. For SS $\rho(r)$ is very close to the case of only one Jupiter discussed above. This result is natural since its mass is dominant in SS. For SMBH galaxy we also find a similar distribution (see Fig. 4) with a slightly slower decay of $\rho_v(r)$ with r ($\beta = 2.06 \pm 0.002$) due to contribution of a larger number of stars. We obtain $\zeta = 3000$ (SS) and $\zeta_g = 3 \times 10^4$ (SMBH). These two examples show that a model of two-body galaxy captures the main physical effects of DMP capture and evolution.

7 DISCUSSION

Our results show that DMP capture and dynamics inside two-body and few-body galaxies can be efficiently described by symplectic maps. The numerical simulations and analytical analysis show that in a center of galaxy the DMP volume density can be enhanced by a factor $\zeta_g \sim 10^4$ compared to its inter-galactic value. The values of ζ_g are maximal for high velocity v_p of planet/star rotating around galactic center.

REFERENCES

Bertone G., Hooper D., Silk J., 2005, Phys. Rep. 405, 279
Casati G., Guarneri I., Shepelyansky D.L., 1987, Phys. Rev. A 36, 3501
Casati G., Guarneri I., Shepelyansky D.L., 1990, Physica A 163, 205
Chirikov B.V., 1979, Phys. Rep. 52, 263
Chirikov B.V., Vecheslavov V.V., 1989, Astron. Astrophys. 221, 146
Galvez E.J., Sauer B.E., Moorman L., Koch P.M., Richards D., 1988, Phys. Rev. Lett. 61, 2011
Garrett K., Dũda G., 2011, Adv. Astronomy 2011, 968283
Khriplovich I.B., Shepelyansky D.L., 2009, Int. J. Mod. Phys. D 18, 1903
Lages J., Shepelyansky D.L., 2013, MNRAS Lett. 430, L25
Malyshkin L., Tremaine S., 1999, Icarus 141, 341
Merritt D., 2010, in Particle Dark Matter: Observations, Models and Searches, Ed. G.Bertone, Cambridge Univ. Press, Cambridge, UK
Peter A.H.G., 2009, Phys. Rev. D 79, 103531; **ibid.** 79, 103533
Petrosky T.Y., 1986, Phys. Lett. A 117, 328
Poincaré H., 1890, Acta Mathematica 13, 1
Rubin V.C., Ford W.K. Jr. Thonnard N., 1980, Astrophys. Jour. 238, 471
Shepelyansky D.L., 2012, Scholarpedia 7(1), 9795
Sivertsson S., Edsjö J., 2012, Phys. Rev. D 85, 123514
Zwicky F., 1933, Helvetica Physica Acta 6, 110